Green Chemistry

PAPER

View Article Online
View Journal | View Issue

Cite this: *Green Chem.*, 2014, **16**, 4292

Mesoporous carbon–silica solid acid catalysts for producing useful bio-products within the sugar-platform of biorefineries†

Patrícia A. Russo,‡[a] Margarida M. Antunes,‡[a] Patrícia Neves,[a] Paul V. Wiper,[a] Enza Fazio,[a] Fortunato Neri,[b] Francesco Barreca,[b] Luís Mafra,[a] Martyn Pillinger,[a] Nicola Pinna*[c] and Anabela A. Valente*[a]

Received 4th June 2014,
Accepted 2nd July 2014

DOI: 10.1039/c4gc01037j

www.rsc.org/greenchem

Useful bio-products are obtainable *via* the catalytic conversion of biomass or derived intermediates as renewable carbon sources. In particular, furanic ethers and levulinate esters (denoted bioEs) have wide application profiles and can be synthesised *via* acid-catalysed reactions of intermediates such as fructose, 5-hydroxymethyl-2-furaldehyde (HMF) and furfuryl alcohol (FA) with ethanol. Solid acid catalysts are preferred for producing the bioEs with environmental benefits. Furthermore, the versatility of the catalyst in obtaining the bioEs from different intermediates is attractive for process economics, and in the case of porous catalysts, large pore sizes can be beneficial for operating in the kinetic regime. Carbon-based materials are attractive acid catalysts due to their modifiable surface, *e.g.* with relatively strong sulfonic acid groups (SO_3H). Considering these aspects, here, we report the preparation of mesoporous (SO_3H)-functionalised-carbon/silica (C/S) composites with large pores and high amounts of acid sites (up to 2.3 mmol g^{-1}), and their application as versatile solid acid catalysts for producing bioEs from fructose, HMF and FA. The mesoporous composites were prepared by activation of an organic compound deposited on the ordered mesoporous silicas MCF (mesostructured cellular foam) and SBA-15, where the organic compound (*p*-toluenesulfonic acid) acted simultaneously as the carbon and SO_3H source. The atomic-level characterisation of the acid nature and strengths was performed by ^{31}P solid-state NMR studies of an adsorbed base probe, in combination with FT-IR and XPS. Comparative catalytic studies showed that the C/S composites are interesting catalysts for obtaining bioEs in high yields, in comparison with classical solid acid catalysts such as sulfonic acid resin Amberlyst™-15 and nanocrystalline (large pore) zeolite H-beta.

Introduction

Concerns about the diminishing reserves of crude oil and the worldwide socio-economic dependence on fossil fuels, as well as the effects of anthropogenic CO_2, are stimulating the development of alternative routes to chemicals and fuels. Special attention is being paid to biomass as a renewable and abundant carbon source, particularly non-edible lignocellulosic biomass which can be obtained from forest, agricultural, municipal and industrial wastes.[1–9] Lignocellulosic matter is composed of lignin and carbohydrate polymers, the latter representing the major portion. Carbohydrates can be chemically transformed into various useful bio-products (denoted bioEs) such as alkyl levulinates (ALs) and the furanic ethers 5-(alkoxymethyl)-2-furfural (5AMF) and 2-(alkoxymethyl)-furan (2AMF) (Scheme 1). ALs find applications in different sectors of the chemical industry, *e.g.* as bio-solvents, plasticizing agents, odorous substances, (bio)fuel additives and as building blocks for chemical transformations.[10,11] In particular, ethyl levulinate (EL)[12–15] and 5-(ethoxymethyl)-furfural (5EMF)[16] possess interesting properties such as oxygenated fuel extenders for gasoline, diesel and biodiesel (*e.g.* to improve engine efficiency, reduce pollutant emissions, *etc.*).

The furanic ethers 5AMF and 2AMF can be synthesised *via* the acid-catalysed reactions of 5-hydroxymethyl-2-furaldehyde (HMF)[17–28] or furfuryl alcohol (FA), respectively, with aliphatic alcohols;[29–34] HMF and FA are derived from the catalytic conversion of hexose and pentose-based carbohydrates, respectively (Scheme 1). The HMF and FA routes can additionally lead

[a]*Department of Chemistry, CICECO, University of Aveiro, Campus de Santiago, 3810-193 Aveiro, Portugal. E-mail: atav@ua.pt*
[b]*Università degli Studi di Messina, Dipartimento di Fisica e di Scienze della Terra, Viale F. Stagno d'Alcontres, 31 98166 Messina, Italy*
[c]*Institut für Chemie, Humboldt Universität zu Berlin, Brook-Taylor-Straße 2, 12489 Berlin, Germany. E-mail: nicola.pinna@hu-berlin.de*
†Electronic supplementary information (ESI) available. See DOI: 10.1039/c4gc01037j
‡These authors contributed similarly to this work.

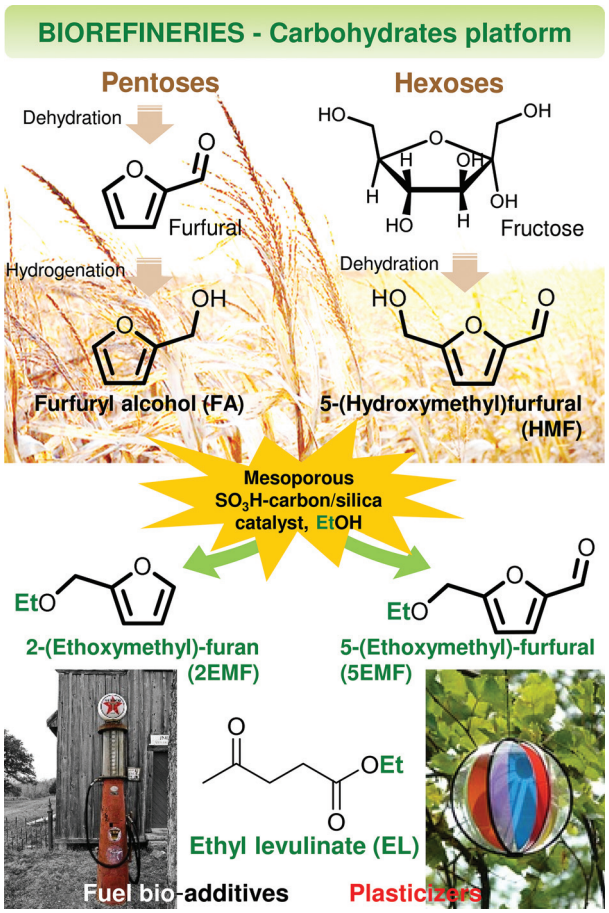

Scheme 1 Envisioned bio-based products of carbohydrates platform biorefineries.

to ALs. Different types of acid catalysts have been investigated for producing bioEs. Homogeneous catalysts, such as mineral and organic acids, inorganic salts, ionic liquids and heteropolyacids, effectively catalyse the reactions of saccharides,[19,24,35–41] HMF[18–20,22–24,36,42] and FA[20,29,32,43,44] to 5AMF, 2AMF and ALs. However, heterogeneous acid catalysts have several advantages over homogeneous ones, such as facilitated separation from the reaction mixture and adequacy for continuous processes.

Commercial ion-exchange resins such as Amberlyst™-15 are amongst the most active solid acid catalysts for producing bioEs from saccharides,[19,25,37,45–49] HMF[19,21,28,50] or FA.[19,29,31–33,51] These types of acid resins possess strong sulfonic acid groups, although their relatively low thermal stabilities can limit catalytic applications. Sulfonated carbon-based materials are expected to be more stable and economical than acid resins. For these reasons, several carbon-based materials including ordered mesoporous carbons,[52,53] graphene-related materials,[54,55] carbon nanotubes,[53,54] carbon–silica composites[56–61] or carbons prepared by incomplete carbonization of organic compounds[62–64] have been modified with SO_3H functionalities and tested as acid catalysts. Indeed, graphene-related materials, carbon–silica composites and carbons produced by sulfonation of incompletely carbonized organics have shown very promising catalytic activity in acid-catalysed reactions of biomass in comparison with commercial catalysts such as zeolites or Amberlyst-15.[54,58,62,65]

Carbon-ordered mesoporous silica composites are particularly interesting materials for the production of SO_3H-functionalised catalysts for biomass conversion. These solids combine the attractive characteristics of ordered mesoporous silicas for catalytic applications, namely, high surface areas, pore volumes and tunable pore sizes, with the attractive properties of the carbon, specifically the high stability for liquid-phase reactions and easily modifiable surface.[56,57,61,66] Further advantages may also arise from the combination of both materials, such as improved hydrothermal and mechanical stability with respect to carbon materials.[67] Moreover, it has been found that stronger acid sites or a higher proportion of stronger acid sites can be created when the carbon is deposited on silica, *i.e.*, stronger solid acids are produced.[56,65] Nevertheless, mesoporous carbon–silica composites have been poorly explored as catalysts for biomass reactions, particularly for the conversion of saccharides, HMF and FA to bioEs.

We have recently reported a simple method for preparing stable SO_3H-functionalised carbon-based materials with high acid site content and strong acidity, which involves the low temperature activation of a carbon precursor that also contains the SO_3H functionality (*p*-toluenesulfonic acid).[65] It was found that a stronger solid acid with improved catalytic activity compared to the pure carbon was obtained when the carbon was deposited on non-porous silica nanoparticles. Herein, we explore this approach and the large surface areas and pore volumes of SBA-15 and mesostructured cellular foam (MCF) silicas to produce mesoporous carbon–silica acid catalysts with relatively high carbon, sulfur and acid sites content, in addition to large pores and strong acid sites. The atomic-level characterisation of acid sites and strengths was achieved by the ^{31}P solid-state NMR studies of adsorbed triethylphosphine oxide (TEPO) in combination with FT-IR and XPS. The composites were effective catalysts in the reactions of HMF and FA with ethanol to give bioEs, as well as in the cascade reaction of fructose–HMF–bioEs; their catalytic performances were compared with those of the commercial catalysts Amberlyst™-15 and nanocrystalline zeolite beta.

Results and discussion

Characterisation

Mesoporous SO_3H-functionalised carbon–silica composites with varied carbon content were prepared by activation of *p*-toluenesulfonic acid deposited into the pores of SBA-15 and MCF silicas (Table 1). The SBA-15 has cylindrical pores of 9.1 nm diameter whereas the MCF consists of 31.5 nm spherical pores accessible through 19.9 nm windows. Therefore, composites with cylindrical mesopores (C/SBA(14), C/SBA(45)) or large spherical mesopores (C/MCF(40), C/MCF(63)) were produced (*cf.* TEM images in Fig. S1†), where the number in parentheses is the wt% of functionalised carbon. Moreover,

Table 1 Chemical and textural characteristics of the mesoporous carbon/silica composites

Sample	R^a	Coating^b (wt%)	S^c (mmol g^{-1})	Acid sites^d (mmol g^{-1})	$S_{BET}{}^e$ (m^{2}g^{-1})	$V_p{}^f$ (cm^{3}g^{-1})	$D_p{}^h$ (nm)
SBA-15	—	—	—	—	793	1.10 (0.05)^g	9.1
MCF	—	—	—	—	668	2.30 (0.03)^g	31.5 (19.9)^i
C/SBA(14)	1.6	14	0.8	1.0	602	0.95	9.1
C/SBA(45)	1.5	45	2.1	1.9	238	0.27	7.6
C/MCF(40)	1.0	40	2.0	1.9	279	0.87	30.4 (17.3)^i
C/MCF(63)	1.6	63	2.2	2.3	198	0.39	22.9 (10.9)^i

^{a} H_2SO_4/TsOH (w/w) ratio. ^{b} Weight% of the functionalised carbon component assessed by TGA. ^{c} Sulfur content determined by elemental analysis. ^{d} Amount of acid sites measured by acid–base titration. ^{e} BET surface area. ^{f} Pore volume. ^{g} Micropore volume in parentheses. ^{h} Pore diameter. ^{i} Window width in parentheses.

the large pore sizes and volumes of the parent silicas enabled the deposition of large quantities of carbon inside the pores.

The Raman spectra of the materials exhibit the D and G bands associated with sp^2 carbon, at *ca*. 1360 and 1580 cm^{-1} respectively (Fig. S2†). The ratio of the peak intensities (I_D/I_G) is *ca*. 0.68 for all samples and indicates that the carbon has very small domains of aromatic rings.[68] The ^{1}H–^{13}C CP MAS NMR spectrum of C/MCF(63) (Fig. S3†) is similar to those reported previously for the materials synthesised using non-porous silica as a support.[65] A main resonance appearing at 129 ppm is assigned to polycyclic aromatic carbons, and two weaker resonances at 20 and 139 ppm are due to methyl groups and carbon bonded to sulfur atoms, respectively.

The wide angle X-ray diffractograms show a single broad reflection at *ca*. 22° 2θ that is typical of the amorphous carbon, overlapped with the contribution from the amorphous silica at similar angles (Fig. S4†). The small angle XRD patterns of C/SBA(14) and C/SBA(45) show reflections associated with the hexagonal arrangement of pores, typical of SBA-15 (Fig. 1). The patterns exhibit the same number of peaks as that of the uncoated silica, which correspond to identical values of the unit cell parameter. Hence, the incorporation of the carbon occurred without significant modification of the pore structural order.

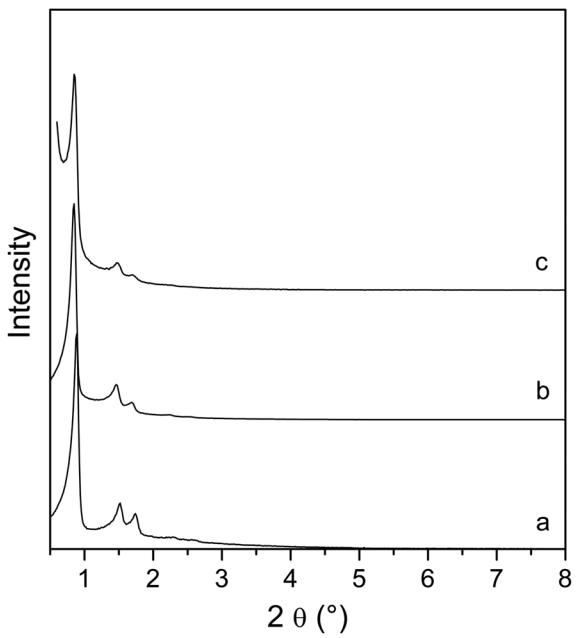

Fig. 1 Small angle X-ray diffractograms of SBA-15 (a), C/SBA(14) (b) and C/SBA(45) (c).

The nitrogen sorption isotherms of both the composites and parental silicas are type IV, with condensation steps and hysteresis cycles at high pressures that reflect the presence of large mesopores in the materials (Fig. 2). The textural properties of the composites depend on their carbon content and on the starting silica (Table 1). Those with the highest carbon contents have the lowest S_{BET}, V_p and D_p compared to the corresponding uncoated silica. None of the composites contain micropores accessible to N_2, which contrasts with the silicas, indicating that the micropores located on the mesopore walls of the silica were filled with carbon. The results suggest that the carbon was successfully deposited inside the mesopores instead of being exclusively deposited on the external surface, which would have completely blocked the porosity of the silica and resulted in non-porous composites with a very low surface area. This can be attributed to the ability of the TsOH molecules to adsorb on the pores, which has been exploited by other authors for the synthesis of ordered mesoporous carbons.[69] Moreover, the incorporation of high quantities of functionalised carbon did not lead to mesopore blocking, therefore the carbon must be fairly well dispersed on the silica pore walls of C/SBA(45), C/MCF(40) and C/MCF(63).

The thickness of the carbon coating can be estimated from the difference between the pore size of the composite and uncoated silica. The carbon content of C/SBA(14) is insufficient to cause a measurable change of pore size. Considering that part of the carbon in this sample is filling the micropores of the silica, most probably a significant portion of the mesopore surface is not covered with carbon. The estimated thicknesses of the coatings of C/SBA(45) and C/MCF(63) are 1.5 nm and 8.6 nm, respectively. For C/MCF(40), values of 1.1 and 2.6 nm are obtained from the difference between the pore sizes and window sizes, respectively. Hence, thicker carbon layers were formed near the windows during the synthesis of C/MCF(40). The coating thicknesses in C/SBA(45) and C/MCF(63) are also not entirely uniform, as indicated by the less

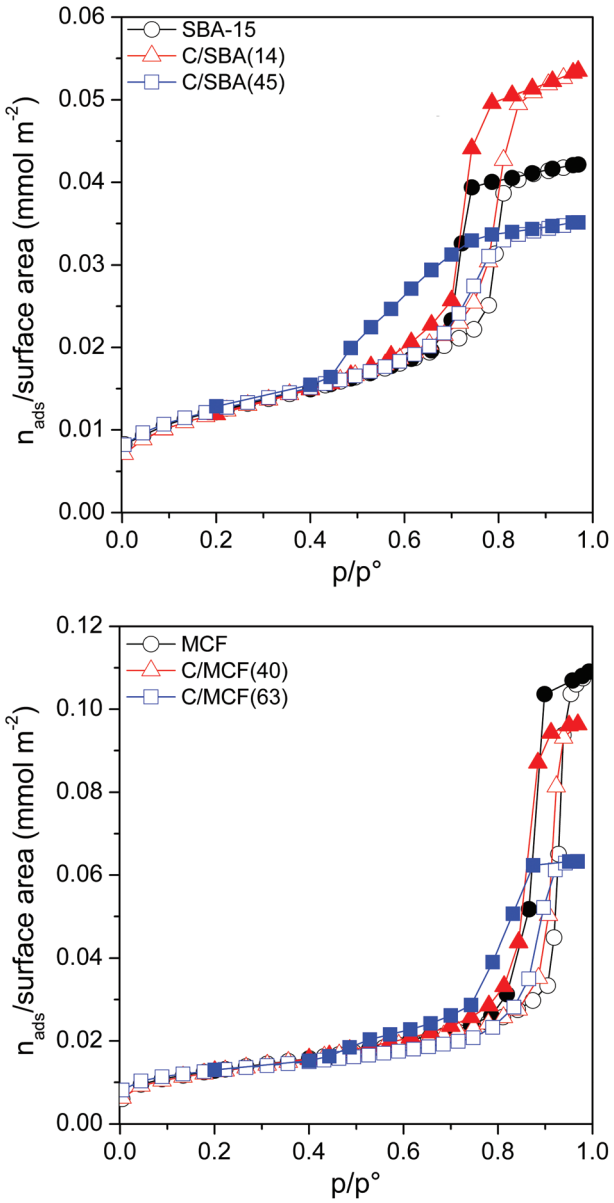

Fig. 2 Nitrogen adsorption–desorption isotherms at −196 °C of the C/S composites and corresponding uncoated silicas, plotted as amount adsorbed per unit of surface area (open symbols – adsorption; closed symbols – desorption).

steep condensation steps on their isotherms compared to those on the corresponding uncoated silicas (Fig. 2). Furthermore, desorption from the mesopores of C/SBA(45) occurs over a wide range of $p/p°$, and the desorption branch of the C/MCF(63) isotherm comprises two steps. The step at higher $p/p°$ is associated with desorption from the mesopores accessible through 10.9 nm windows, whereas the small step at lower $p/p°$ corresponds to mesoporosity accessible through narrower regions (*ca.* 4–5 nm), which however only accounts for less than 10% of the total pore volume of the sample. This means that the non-uniformity of the carbon layer creates narrowed regions inside the mesopores of C/SBA(45) and C/MCF(63). Nevertheless, most of these narrower regions have sizes in the mesopore range and thus are not expected to hinder diffusion through the pores.

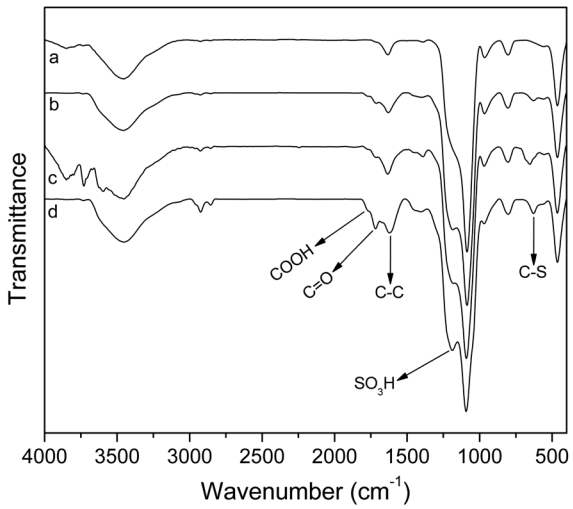

Fig. 3 FT-IR spectra of (a) C/SBA(14), (b) C/SBA(45), (c) C/MCF(40) and (d) C/MCF(63).

The FT-IR spectra of the composites (Fig. 3) exhibit bands at 1090, 960, 804 and 464 cm^{-1} arising from the silica component of the materials (the spectra of the parent silicas are shown in Fig. S5 of ESI†). Additionally, the spectra of C/SBA(45), C/MCF(40) and C/MCF(63) show bands associated with the carbon and its functional groups. Specifically, the bands at 1777, 1719 and 1390 cm^{-1} indicate the presence of carboxylic acid, ketone and hydroxyl functional groups, respectively, whereas those at 1183 and 625 cm^{-1} are associated with the SO_3H groups bonded to the carbon. The COOH, C=O and C–OH functional groups are produced by oxidation of the carbon by the small amounts of sulfuric acid used for the synthesis. The band at 1600 cm^{-1} is ascribed to the skeletal vibrations of the C–C bonds. The carbon-related bands are not clearly visible in the spectrum of C/SBA(14), due to the low carbon content of this sample and low intensity of its bands compared to those of silica.

X-ray photoelectron spectroscopy (XPS) analysis was performed to gain additional information on the surface composition of the composites (Fig. 4). The S 2p spectra have two contributions at 164 and 169 eV associated with sulfur in SH and SO_3H groups, respectively,[70] with most of the sulfur belonging to the latter. C/MCF(63) has the highest relative amount of SO_3H (82.8%), followed by C/MCF(40) and C/SBA(45), both containing similar relative amounts (>71%). These results contrast with the complete absence of SO_3H found for TsOH carbonized at higher temperature,[69] and can be attributed to the low temperature activation process used here. The C 1s regions are composed of four contributions at 284.6, 286.3, 287.7 and 289.1 eV ascribed to C–C, C–O (as in C–OH), C=O and COOH, respectively.[71,72] The percentage of C–O bonding decreases in the following order C/MCF(40) > C/SBA(14) > C/MCF(63) > C/SBA(45) (Table S1†). Neither the C–O bonding percentage nor the SH/SO_3H ratio is directly correlated with

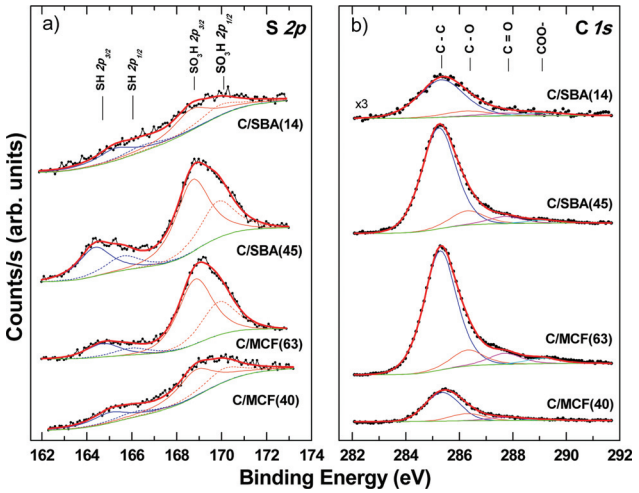

Fig. 4 (a) S 2p and (b) C 1s X-ray photoelectron spectra of the mesoporous C/S composites.

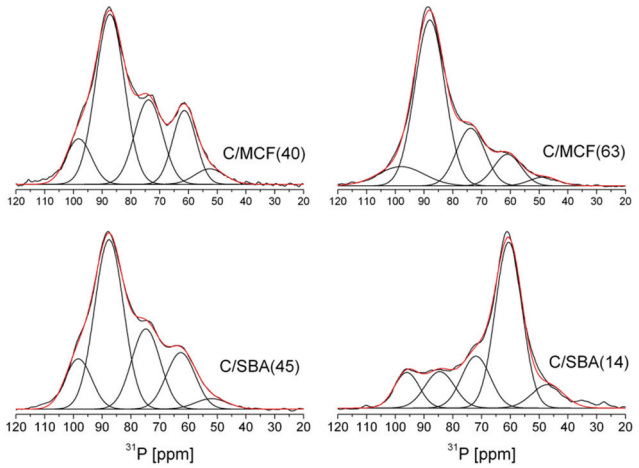

Fig. 5 ^{1}H-decoupled ^{31}P MAS NMR of the mesoporous C/S composites.

the H_2SO_4/TsOH mass ratio used for the synthesis (Tables 1 and S1†), in contrast to what was found when non-porous silica particles were used as a support.[65] Hence, other factors, such as the amount, location and dispersion of the carbon inside the pores, seem to play a role on the final surface composition of the materials. The relatively high surface Si/C and O/C ratios of C/SBA(14) confirm that a significant part of the silica surface is not covered with carbon (Table S2†).

The FT-IR and XPS results discussed above show that the materials have several types of surface acidic functionalities such as SO_3H, COOH and C–OH, which means that the acid sites quantified by titration correspond to the total amount of acidic groups (Table 1). The composites with the highest carbon contents exhibit higher amounts of sulfur and acid sites. The amount of acid sites decreases in the following order C/MCF(40) > C/MCF(63) ≈ C/SBA(45) ≫ C/SBA(14). Since part of the pore surface of C/SBA(14) is not coated with carbon, the total acid sites of this sample, measured by titration, possibly includes weak silanol groups. Comparison of the acid sites and S contents of each sample, together with the fact that the acid sites content include acid groups other than SO_3H, suggest that a portion of the sulfur of the samples is not included in surface acidic groups. Some of the sulfur belongs to SH groups and may also be in the bulk. It is worth mentioning that using silicas with large pores and pore volumes it was possible to produce materials with higher amounts of S and acid sites than those prepared by coating silica nanoparticles.[65] Interestingly, most of the composites also contain significantly higher S and/or acid sites content than similar materials reported in the literature.[56,58,59,61] This is because the carbon precursor molecule has SO_3H groups in its composition. In contrast, the common methods for synthesising this type of material first involves the carbonization of a carbon precursor deposited inside the pores followed by a sulfonation procedure (*e.g.* with concentrated H_2SO_4).[56,58,59,61]

The acid strength was qualitatively assessed by observing the ^{31}P chemical shifts of adsorbed triethylphosphine oxide (TEPO); the higher the chemical shift value, the stronger the acid site.[73] The ^{31}P MAS NMR spectra of the composites exhibit broad line-shapes indicating a distribution of acid sites (Fig. 5). In order to facilitate comparisons between the samples the spectra were deconvoluted and fitted using five Gaussian components centered at *ca.* 98, 87, 74, 61 and 52 ppm (Table S3†).

The TEPO ^{31}P chemical shifts indicate that all of the composites possess acid sites ranging from very strong (96–98 ppm), strong (88 ppm), medium (74 ppm) to weak (61 ppm) acidity. The resonance at *ca.* 52 ppm is due to physisorbed TEPO species.[74] The XPS and FT-IR results revealed that the composites have several types of acidic functionalities with different acid strengths. Hence, combining the results from XPS and FT-IR with the ^{31}P chemical shift ranges of adsorbed TEPO, we assign the resonances at 61 and 74 ppm to TEPO interacting with the relatively weak OH and COOH groups, whereas the higher chemical shift at 88 ppm is associated with stronger SO_3H groups. We also tentatively assign the resonance at *ca.* 98 ppm to sulfuric acid ester groups, which are expected to be stronger than SO_3H. The resonance at 61 ppm dominates the spectrum of C/SBA(14), which is explained by a high portion of the silica being uncoated by carbon and consequently the surface of this sample contains a significant amount of weakly acidic silanol groups. C/MCF(63) contains the highest relative amount of the strongest acid sites (resonances at 98 and 88 ppm), followed by C/MCF(40) and C/SBA(45), which have acid sites of similar strength, consistent with the results obtained from XPS. The spectrum of the benchmark acid catalyst Amberlyst™-15 displays a single resonance at 90.5 ppm.[54] This means that our catalysts have acid sites of weaker, comparable strength and also a small amount of stronger acid sites than the acid resin.

Catalytic studies

Reaction of HMF to bioEs. The reaction of HMF in the presence of the carbon (C/S) composites gave 5EMF and EL (bioEs denotes 5EMF plus EL) as the main products in total yields of

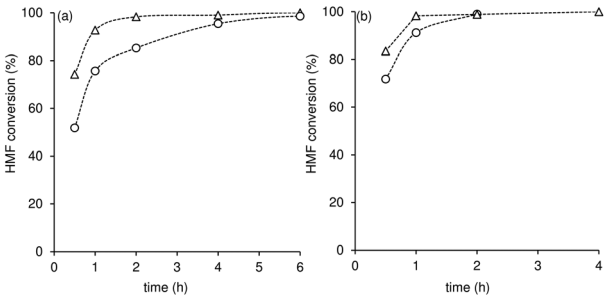

Fig. 6 Kinetic profiles of the reaction of HMF with ethanol in the presence of composites (a) C/SBA-15 (C/SBA(45) (Δ), C/SBA(14) (O)) or (b) C/MCF (C/MCF(63) (Δ), C/MCF(40) (O)). Reaction conditions: 0.33 M HMF, catalyst loading = 10 g_{cat} dm^{-3}, 110 °C. The dashed lines are visual guides.

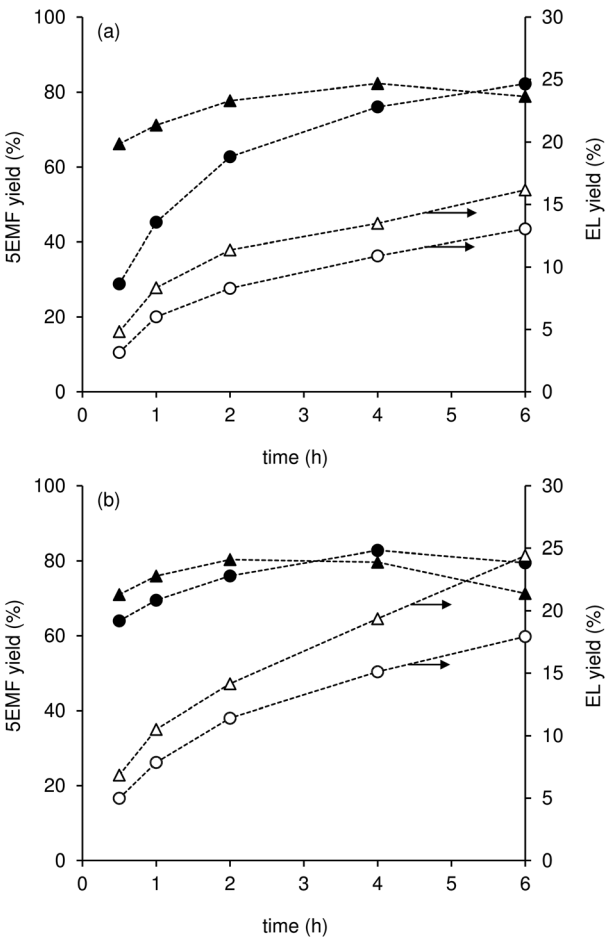

Fig. 7 Dependency of the yields of 5EMF (black symbols) and EL (white symbols) on the time of reaction of HMF in the presence of the composites (a) C/SBA-15 ((C/SBA(45) (triangles), C/SBA(14) (circles)) or (b) C/MCF ((C/MCF(63) (triangles), C/MCF(40) (circles)). Reaction conditions: 0.33 M HMF, catalyst loading = 10 g_{cat} dm^{-3}, 110 °C. The dashed lines are visual guides.

95–99% within 2–6 h reaction at 110 °C (conversion >99%; Fig. 6 and 7). The reaction mechanism of HMF to EL is complex and involves the intermediate formation of 5EMF which was the main product formed initially (80–83% yield at 2–6 h). The conversion of 5EMF to EL is favoured by strong Brønsted acidity.[21,26] Hence, our strongest solid acid catalyst C/MCF(63) was the most effective for producing EL; 42% EL yield compared to 23–29% for the remaining catalysts, at 100% conversion and 24 h (Fig. 7 and S6†).

For each pair of C/S composites with the same silica support, the catalyst with the highest total amount and strength of acid sites (AcS) led to faster initial reaction of HMF and higher yield of bioEs (*i.e.* C/MCF(63) and C/SBA(45) in comparison with C/MCF(40) and C/SBA(14), respectively, Fig. S7†). The differences in catalytic results were more pronounced for the C/SBA-15 composites than for the C/MCF ones, most likely due to the larger differences of acid properties in the former case. On the other hand, for each pair of C/S composites with the same silica support, the more active catalyst (Fig. 6 and S7†) possessed lower specific surface area, pore volume and sizes (Table 1) than the less active one (*i.e.* C/SBA(45) and C/MCF(63) in comparison with C/SBA(14) and C/MCF(40), respectively). Hence, the acid properties of the C/S catalysts seem to play a major role in the catalytic reaction, and, on the other hand, suggest good active site accessibility with the texture properties not causing significant constraints on the catalytic reaction (*i.e.* the catalytic reaction systems are likely operating under the kinetic regime). This hypothesis is further supported by a comparison of the catalytic performances of C/S materials with similar acid properties, but different structural/textural properties, namely, C/MCF(40) and C/SBA(45). The C/MCF(40) material has a much higher mesoporous volume (*ca.* three times greater) and larger pores (*ca.* six times greater) than C/SBA(45). Despite the differences in textural/structural properties, the two composites led to similar catalytic results, which correlate with their similar acid properties (Fig. S8†).

The catalytic performances of C/MCF(63) and C/SBA(45) compare favourably to various carbon-based materials previously tested as catalysts in the same reaction under similar conditions, namely, sulfonated partially reduced graphene oxide,[54] sulfonated carbon nanotubes,[54] sulfonated carbon black,[54] and non-porous silica nanospheres coated with sulfonated carbon (Table 2).[65] The same applies when comparing the C/S catalysts to microporous crystalline or mesoporous amorphous aluminosilicates, such as nanocrystalline zeolite H-beta (as determined by catalytic tests carried out under similar reaction conditions, Fig. S9†) and mesoporous Al-TUD-1.[33]

The catalytic performances of the C/S composites were further compared to that of the classical catalyst Amberlyst™-15 which possesses a macroreticulated polymer matrix functionalised with sulfonic acid groups. These types of resins are very active catalysts for the conversion of furanic compounds (HMF, FA) to bioEs, and are thus good benchmark catalysts.[18,19,21,25,28,29,31–33,50] The texture properties and the acid sites accessibility of the acid resins depend on their swelling ability in the liquid media. In order to minimise the swelling effects, Amberlyst™-15 was ground into a very fine powder

Table 2 Comparison of the catalytic results for the C/S catalysts with those of various other catalysts tested in the reaction of HMF with ethanol

	Reaction conditions[b]						
Catalyst[a]	T (°C)	$[HMF]_0$ (M)	Cat. load (g_{cat} dm^{-3})	t (h)	Conv.[c] (%)	bioEs yield (%)	Ref.
C/SBA(45)	110	0.33	10	2/4	98/99	89/96	—
C/MCF(63)	110	0.33	10	2/4	99/100	95/99	—
CST-1	110	0.33	10	2/4	92/99	84/97	65
S-RGO	110	0.33	10	4	98	96	54
S-GO	100	0.5	10	12	85	83	50
S-CNT	140	0.33	10	24	99	86	54
S-CB	140	0.33	10	24	99	85	54
Amberlyst-15	110	0.33	10	2/4	95/99	75/85	65
H-Beta	110	0.33	10	6	73	78	—
Al-TUD-1(21)	110	0.3	10	4	98	96	33
Al-MCM-41(25)	140	0.7	n.m.	5	100	84	21
Al-MCM-41(50)	140	0.7	n.m.	5	100	78	21
ZrO_2/SBA-15	140	0.7	n.m.	5	100	99	21
SO_4^{2-}/ZrO_2/SBA-15	140	0.7	n.m.	5	100	97	21
SO_3H-SBA-15	140	0.12	16	24	~100	~85	26
HMS-SO_3H	100	0.20	200	10	95	85	83
H-ZSM-5 (11.5)	140	0.12	16	24	~100	~87	26
H-Mordenite(10)	140	0.12	16	24	~100	~85	26
Silica sulfuric acid	75	0.39	4.3	24	100	68	19
H-Y	70	0.2	6	24	10	9	22
$H_4SiW_{12}O_{40}$/MCM-41	90	1.7	42	4	92	82	18

[a] Value in parenthesis (when applied) is the Si/Al molar ratio. [b] Reaction conditions: T = reaction temperature (°C), $[HMF]_0$ = initial molar concentration of HMF, Cat. load = catalyst loading, t = time of reaction (h), n.m. = not mentioned. [c] HMF conversion.

with particle sizes of a few hundreds of nanometers, and tested in the reaction of HMF under similar conditions. The resin catalyst led to slower conversion of HMF to bioEs than our strongest acid C/S catalysts; conversion at 30 min was 53% for the resin catalyst,[65] compared to 74% and 83% for C/SBA-(45) and C/MCF(63), respectively (Fig. 6), and the bioEs yield at 30 min was 46% for the resin catalyst,[65] compared to 71% and 78% for C/SBA(45) and C/MCF(63), respectively (Fig. S7†). In this case, the catalytic activity does not correlate with the amount of acid sites which is higher for the acid resin catalyst (4.3 $mmol_{SO_3H}$ g^{-1}).[65] Possibly, the resin catalyst possesses some acid sites which are inaccessible and/or subject to important steric hindrance effects in their vicinity. The good catalytic performances of the strongest acid C/S catalysts may be partly due to their favourable acid properties and good active site accessibility. Using a greater initial amount of HMF (*ca.* 3.9 times greater than the typical conditions) and less solvent (half the amount), the C/MCF(63) catalyst, for example, still led to fairly good catalytic results (Fig. S10†). For the more concentrated HMF reaction conditions, the composite catalyst led to faster initial conversion of HMF to bioEs (61% yield at 74% conversion and 30 min reaction) than Amberlyst™-15 using less concentrated HMF reaction conditions (46% yield at 53% conversion).[65]

Reaction of fructose to bioEs. The mesoporous composites C/MCF(63) and C/SBA(45) were further explored as catalysts for the cascade reaction of fructose to bioEs in a single reactor, at 140 °C (Fig. 8). The acid-catalysed dehydration of fructose gives HMF, which is subsequently converted to bioEs. For the two catalysts, the main products were HMF and bioEs, formed in maximum yields of 39% (at 83–85% conversion and 4–6 h reaction) and 44–48% (at 100% conversion and 24 h reaction), respectively. The C/MCF(63) catalyst led to faster reaction of HMF than C/SBA(45), which correlates with the higher total amount of acid sites for the former. The higher initial reaction rate for C/MCF(63) was accompanied by higher initial yield of the intermediate product HMF, and higher bioEs yields were reached with time in relation to C/SBA(45). The C/MCF(63) catalyst led to higher EL yield than C/SBA(45) (21% and 15%, respectively, at 48 h reaction), and this trend parallels that observed for HMF as a substrate using the two catalysts (Fig. 7 and S6†), and may be partly due to somewhat stronger acidity of C/MCF(63).

The catalytic performances of C/MCF(63) and C/SBA(45) were compared to those of various other solid acid catalysts tested in the same reaction. The two composites led to faster conversion of fructose to bioEs yields than powdered Amberlyst-15 tested at 110 °C (the maximum operation temperature recommended is 120 °C): 44% conversion at 4 h reaction for the resin catalyst compared to 73–83% for the composites, and 9% bioEs yield at 24 h for the resin catalyst compared to 44–48% yield for the composites. Furthermore, the composites led to much faster reaction of fructose than nanocrystalline zeolite H-beta, as determined by catalytic tests carried out under similar reaction conditions (Table 3); 57% conversion at 24 h compared to 100% for the composites. Table 3 summarises literature data for various other solid acid catalysts tested in the one-pot conversion of fructose to BioEs. The C/MCF(63) and C/SBA(45) catalysts led to faster reaction of fructose than non-porous silica nanoparticles coated with

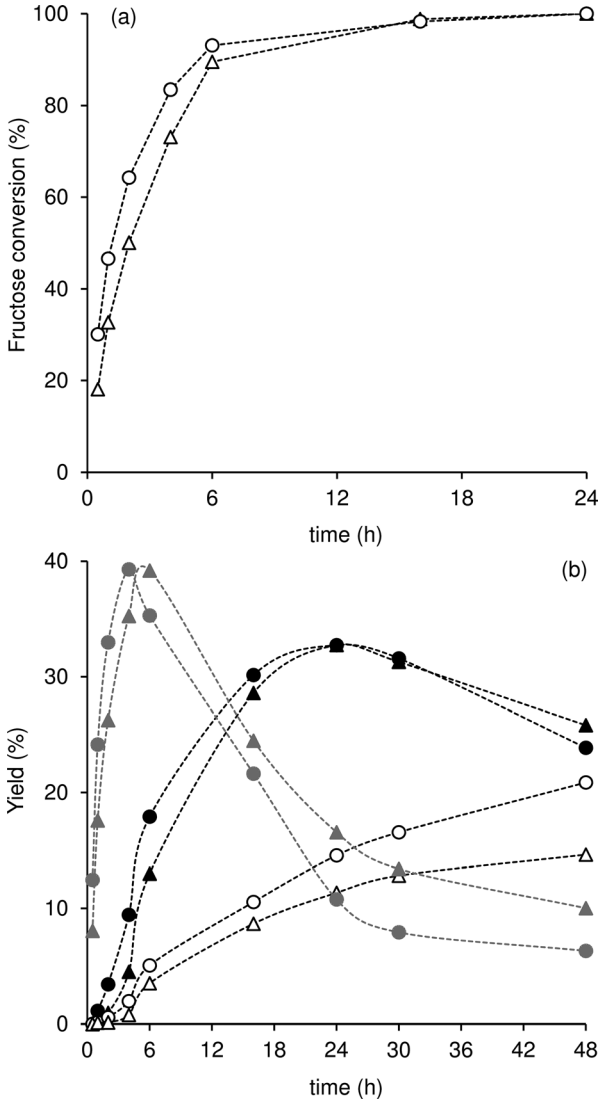

Fig. 8 (a) Kinetic profiles and (b) dependency of the yields of HMF (grey symbols), 5EMF (black symbols) and EL (white symbols) on the time of reaction of fructose in the presence of C/SBA(45) (triangles) or C/MCF (63) (circles). Reaction conditions: 0.33 M fructose, water–ethanol (3 : 7 v/v ratio) solvent mixture, catalyst loading = 10 g_{cat} dm^{-3}, 140 °C. The dashed lines are visual guides.

sulfonated carbon, tested under similar reaction conditions.[65] For various cases, it is difficult to make clear and fair comparisons due to the different reaction conditions used, which can facilitate or not the conversion of HMF to bioEs: in some cases higher EL yields were reported using (i) lower temperature and catalyst loading, despite a lower initial concentration of fructose (CNT-PSSA, BSA and CMK-5-PSSA),[53] or (ii) higher temperature and catalyst loading (*e.g.* zeolites),[26,75] or (iii) higher catalyst loading (SBA-15-SO_3H).[26] On the other hand, for some catalysts higher 5EMF yields were reported using lower temperature, despite lower initial fructose concentration and higher catalyst loading (silica-SO_3H, Fe_3O_4@SiO_2–SO_3H).[76]

Reaction of FA to bioEs. The C/S composites were further explored as acid catalysts for the production of EL *via* an alternative route to that of HMF (hexose route), specifically from FA which is industrially produced from furfural (pentose based route).[77,78] FA has been proven to be an interesting feedstock for levulinate esters production *via* atom-economic methods under relatively mild reaction conditions. Our C/S composites were very active in the reaction of FA, leading to 100% conversion within 30 min, at 110 °C. Initially, FA was converted to 2-(ethoxymethyl)-furan (2EMF) (36–56% yield at 30 min) which was subsequently converted to EL with yields of up to 79% (Fig. 9). Besides EL, the intermediate product 2EMF can find interesting applications such as a pharmaceutical and food additive, and as a blending component of gasoline.[34] Nevertheless, our catalysts favour essentially the formation of EL in the FA reaction system. A comparison of the catalytic results for the two substrates FA and HMF indicates a much higher reactivity of FA in comparison with HMF, and that the FA route leads to higher EL yields. Similar results have been reported in the literature for different materials tested as catalysts in the two reactions.[33,65]

The relationships between the acid properties of the C/S catalysts and the EL yields are similar for the three substrates: HMF (Fig. 7), fructose (Fig. 8) and FA (Fig. 9). For each pair of composites possessing the same ordered mesoporous silica support, a higher total amount of acid sites and stronger acidity favours the formation of EL. Furthermore, the C/MCF(40) and C/SBA(45) catalysts which possess similar acid properties led to similar catalytic results (Fig. S8 and S11†).

Catalyst stability and reusability. The stability of the materials in the reaction media can be assessed by a pre-treatment of the catalysts in the solvent, at the reaction temperature and in the absence of the substrate. Therefore, contact tests in ethanol (ET) were carried out for C/SBA(45) and C/MCF(63), giving the treated solids C/SBA(45)-ET and C/MCF(63)-ET, respectively (for details see the Experimental section). The amounts of sulfur and acid sites of the treated solids did not decrease, suggesting that C/SBA(45) and C/MCF(63) are stable towards leaching of the surface active species. Moreover, FT-IR spectra of the treated solids were similar to those of the corresponding original solids (Fig. S5†). The treated solids were tested as catalysts in the reaction of HMF with ethanol under typical conditions; the catalytic results were similar to those of the corresponding original materials (Fig. 10). Furthermore, the catalytic performances remained similar after subjecting C/SBA(45) and C/MCF(63) to two consecutive treatments in ethanol (C/SBA(45)-ET(2) and C/MCF(63)-ET(2), respectively).

The recovered C/SBA(45) catalyst was reused in a consecutive 6 h batch run, giving high bioEs yield (93%) at high conversion (99%), with higher selectivity to 5EMF than EL (85% 5EMF plus 8% EL yield), similar to that observed for run 1 (79% 5EMF and 16% EL yield at 100% conversion). Similar trends were observed for the original and reused C/MCF(63) catalysts, *i.e.* the recovered catalyst led to high bioEs yield, especially of 5EMF (84% 5EMF and 8% EL yield) at high conversion (99%).

Table 3 Comparison of the catalytic results for the C/S catalysts with those for various catalysts tested in the reaction of fructose using ethanol as a solvent[a]

Catalyst	$[Fru]_0$ (M)	Cat. load (g_{cat} dm^{-3})	Co-solvent	T (°C)	t (h)	Conv. (%)	Y_{HMF} (%)	Y_{EL} (%)	Y_{5EMF} (%)	Ref.
C/SBA(45)	0.33	10	H_2O	140	6/24	89/100	39/17	4/11	13/33	—
C/MCF(63)	0.33	10	H_2O	140	4/24	83/100	39/11	2/15	9/33	—
CST-1	0.33	10	H_2O	140	24	95	28	7	27	65
Amberlyst-15	0.33	10	H_2O	110	4/24	44/72	9/33	0/2	0/7	—
H-Beta (12)[b]	0.33	10	H_2O	140	4/24	31/57	3/9	—/<1	—/6	—
GO	0.5	20	—	100	24	95	9	—	18	50
GO	0.5	30	DMSO	130	24	100	9	—	71	50
CNT-PSSA[c]	0.07	5	—	120	24	>99	—	84	—	53
CNF-PSSA[d]	0.07	5	—	120	24	>99	—	69	—	53
CMK-5-PSSA[e]	0.07	5	—	120	24	>99	—	60	—	53
CNT-BSA[f]	0.07	5	—	120	24	>99	—	45	—	53
Amberlyst-70	0.63	0.13	H_2O	175	1.3	100	0	38	nm	49
Amberlyst-131	0.74	0.13	—	~78	24	95	—	—	62	48
Amberlyst-131	63.6	14.2	—	110	0.75	100	—	21	44	48
Cellulose H_2SO_4	0.2	10	—	100	12	95	nm	13	73	79
Fe_3O_4@SiO_2–SO_3H[g]	0.2	40	—	100	16	97	3	—	72	76
Silica-SO_3H[h]	0.2	40	—	100	24	100	11	—	63	80
SBA-15-SO_3H	0.29	15.7	—	140	24	>99	<1	57	12	26
H-beta (12.5)[b]	0.29	15.7	—	140	24	92	<1	7	26	26
H-Beta (19)[b]	0.1	150	—	160	20	>99	—	48	—	75
H-Y (6)[b]	0.1	150	—	160	20	>99	—	40	—	75
H-Y (2.6)[b]	0.29	15.7	—	140	24	93	<1	8	28	26
H-MOR (10)[b]	0.29	15.7	—	140	24	92	13	—	42	26
H-ZSM-5 (11.5)[b]	0.29	15.7	—	140	24	94	15	—	17	26

[a] Reaction conditions: $[Fru]_0$=initial concentration of fructose, co-solvent (when applied), Cat. Load = catalyst loading, T = reaction temperature, t = reaction time. The results are indicated for fructose conversion (Conv.) and product yield (Y); nm = not mentioned. [b] Values in parenthesis correspond to the Si/Al molar ratio. [c] CNT-PSSA – poly (*p*-styrenesulfonic acid)-grafted carbon nanotubes. [d] CNF-PSSA – poly(*p*-styrenesulfonic acid)-grafted carbon nanofibers. [e] CMK-5-PSSA – benzenesulfonic acid-grafted CMK-5. [f] CNT-BSA – benzenesulfonic acid-grafted carbon nanotubes. [g] Fe_3O_4@SiO_2–SO_3H – sulfonic acid immobilised on the surface of silica-encapsulated Fe_3O_4 nanoparticles. [h] Silica-SO_3H – silica supported sulfonic acid.

In order to confirm the absence of soluble active species, the liquid phase obtained from the contact test of C/SBA(45) with ethanol (denoted C/SBA(45)-ET(liq)) was tested for the homogeneous phase reaction of HMF. The substrate was added to C/SBA(45)-ET(liq) to give 0.33 M HMF, and the resulting solution was left to react at 110 °C for 6 h. The homogeneous phase reaction was sluggish, giving similar HMF conversion (20%) to the reaction of HMF without the catalyst (17%). Hence, the catalytic reaction seems to take place in the heterogeneous phase. In the case of C/MCF(63) it was not possible to confirm the heterogeneous nature by the contact test because the filter used (0.2 μm PTFE membrane) could not completely separate the catalyst particles from the liquid phase. Nevertheless, the conversion was much lower than that observed for the original catalyst (49% at 6 h reaction, compared to 99% at 2 h reaction for C/MCF(63)). On the other hand, as mentioned above no significant changes in the amount of acid sites and S content were observed for C/MCF-(63)-ET, and thus C/MCF(63) seems stable towards leaching. Furthermore, the catalytic performances of C/SBA(45) and C/MCF(63) remained similar after hydrothermal treatment at 140 °C for 24 h (C/SBA(45)-WT and C/MCF(63)-WT, respectively; details in the Experimental section), Fig. 10. The IR spectral features remained similar for all treated solids (Fig. S5†).

Conclusions

Composites (C/S) consisting of mesoporous silicas SBA-15 or MCF coated with carbon functionalised with acidic groups of different strengths (such as SO_3H and COOH) are versatile solid acid catalysts for synthesising useful bio-products. The composites promoted the conversion of different intermediates derived from biomass, namely 5-hydroxymethyl-2-furaldehyde (HMF), fructose and furfuryl alcohol (FA) to the bio-products 5-(ethoxymethyl)-2-furfural (5EMF), 2-(ethoxymethyl)-furan (2EMF) and ethyl levulinate (EL). The composites, which have high total amount of acid sites (up to 2.3 mmol g^{-1}), in addition to large mesopores and some very strong acid sites, were synthesised by the activation of varied amounts of *p*-toluenesulfonic acid deposited on the silicas. The atomic-level characterisation of the acid nature and strengths was performed by ^{31}P solid-state NMR studies of the adsorbed base probe, in combination with FT-IR and XPS. The C/S catalysts with higher acid site contents (1.9–2.3 mmol g^{-1}) and strengths led to higher yields of bioEs in the reactions of HMF (95–99% 5EMF + EL yield within 2–6 h reaction), fructose (44–48% yield of 5EMF + EL, and 11–17% HMF yield at 24 h reaction) and FA (up to 78% yield at 100% conversion). The catalysts were stable towards S leaching and reusable. The performances of the C/S catalysts have been compared to various

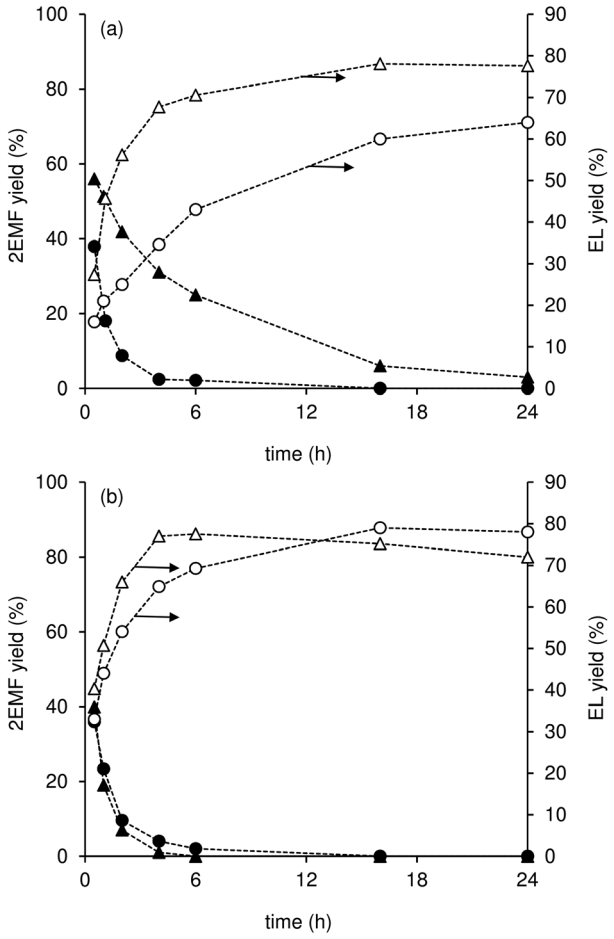

Fig. 9 Dependency of the yields of 2EMF (black symbols) and EL (white symbols) on the time of reaction of FA (until 24 h) in the presence of composites (a) C/SBA-15 (C/SBA(45) (triangles), C/SBA(14) (circles)) or (b) C/MCF (C/MCF(63) (triangles), C/MCF(40) (circles)); FA conversion was always 100%. Reaction conditions: 0.33 M FA, catalyst loading = 10 g_{cat} dm^{-3}, 110 °C. The dashed lines are visual guides.

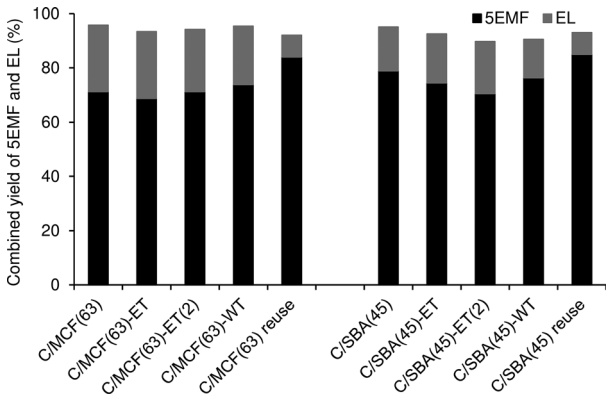

Fig. 10 Catalytic performances of C/MCF(63), C/SBA(45) and the corresponding pre-treated solids (with ethanol once (ET) or twice (ET(2)), or with water (WT)) in the reaction of HMF with ethanol; HMF conversion was at least 98%. Reaction conditions: 0.33 M HMF, catalyst loading = 10 g_{cat} dm^{-3}, 110 °C, 6 h.

other solid acid catalysts. The acid strengths of the C/Ss covered those of the benchmark strong acid catalyst Amberlyst™-15 (a bulk macroreticular sulfonic acid resin), although the distribution of acid strengths was wider and the acid site contents were lower than for the acid resin (4.3 mmol g^{-1}). However, with the C/S catalysts, HMF and fructose were converted to bioEs at higher rates than with Amberlyst™-15 (on the same catalyst mass basis), which may be partly due to favourable texture properties and enhanced active site accessibility of our materials. The catalytic results for the C/S materials compared favourably to those of various carbon-based and aluminosilicate catalysts, such as non-porous silica nanoparticles coated with sulfonated carbon and nanocrystalline zeolite H-beta.

The synthesis of C/S composites from biomass derived components for paving the way towards greener production of bioproducts can be envisaged. Silica and carbon precursors are obtainable from waste products with the increasing use of biomass. For example, biomass fly ash has been used as a silica source for the green synthesis of a nanosilicate.[81] On the other hand, the pulp and paper industry generates lignosulfonate by-products which can be synthetic precursors to the sulfonic acid carbon component; it has been demonstrated that these types of compounds possess catalytic activity in the conversion of HMF to bioEs.[54]

Experimental

Synthesis of the materials

The SBA-15 and MCF silicas were synthesised following procedures reported in the literature.[82–84] Briefly, to synthesise the SBA-15,[82] 4.3 g of tetraethylorthosilicate (TEOS; 98%, Aldrich) was added to 2 g of Pluronic P123 (Aldrich) dissolved in 75 mL of 1.6 M aqueous HCl solution. The mixture was stirred at 40 °C for 20 h, transferred to an autoclave and heated at 100 °C for 2 days. The solid was collected by filtration, washed with distilled water, dried at 65 °C and calcined at 550 °C for 8 h. The MCF silica was synthesised through a similar procedure with some modifications:[82,83] 4.0 g of mesitylene (98%, Aldrich) followed by 23 mg of ammonium fluoride (≥98%, Aldrich) were added to the surfactant solution and the mixture was stirred for 1 h at 40 °C prior to the addition of TEOS (4.3 g). The suspension was aged in an autoclave at 100 °C for 24 h. The solid was recovered by filtration, washed with water, dried at room temperature and calcined at 500 °C for 8 h.

The carbon–silica composites were synthesised by activation of various amounts of *p*-toluenesulfonic acid (TsOH, Panreac) impregnated on 1 g of mesoporous silica. TsOH was dissolved in acetone (99.9%, Aldrich) and added to the silica. The suspension was sonicated for 15 min, stirred for 24 h at room temperature, and then heated at 100 °C for 6 h and for 6 h at 160 °C. The TsOH–silica solid was suspended in 10 mL of aqueous H_2SO_4 solution and stirred for 24 h at room temp-

erature. The concentration of the H_2SO_4 solution was changed in order to obtain the desired H_2SO_4/TsOH mass ratio R (Table 1). After evaporation of water at 110 °C, the acid impregnated solid was heated at 250 °C in a tubular furnace under a N_2 flow for 1 h. The resulting solid was washed with distilled water (until neutral pH) followed by acetone, and dried at 65 °C. The samples are denoted C/SBA(x) or C/MCF(x), where x is the wt% of the functionalised carbon.

Characterisation

The carbon and sulfur contents of the samples were determined by elemental analysis with a TruSpec 630 elemental analyser. Powder X-ray diffraction (XRD) patterns were measured on a PANalytical Empyrean diffractometer at 45 kV and 40 mA using Cu Kα radiation (λ = 0.1541 nm). FT-IR spectra were recorded on a Bruker Tensor 27 spectrometer using pellets of the sample mixed with KBr (400–4000 cm^{-1}, 256 scans, 4 cm^{-1} resolution). Raman measurements were carried out on a JobinYvon T64000 spectrometer (laser λ: 532 nm). X-ray photoelectron spectroscopy (XPS) analysis was performed on a K-Alpha system from Thermo Scientific, equipped with a monochromatic Al Kα source (1486.6 eV), and operating in constant analyser energy (CAE) mode with a pass energy of 200 and 50 eV for survey and high resolution spectra, respectively. A spot size diameter of about 400 μm was adopted. Transmission electron microscopy (TEM) images were recorded with a JEOL 2200FS microscope at 200 kV. Nitrogen adsorption isotherms at −196 °C were measured with a Micromeritics Gemini 2380, after degassing of the samples at 120 °C overnight. The surface areas were calculated with the Brunauer–Emmett–Teller (BET) equation; pore volumes were calculated with the α_s method; pore sizes were calculated with the DFT method. Thermogravimetric analyses (TGA) were performed under air flow from room temperature to 700 °C, with a heating rate of 5 °C min^{-1}, on a Shimadzu TGA-50. The total acid sites content was measured by acid–base titration: the sample (0.1–0.2 g) was stirred at room temperature for 24 h in 20 mL of 0.1 M NaCl, and then titrated with 0.01 M NaOH. The acid strength of the solids was evaluated by ^{31}P MAS NMR of chemically adsorbed triethylphosphine oxide (TEPO). The adsorption of TEPO was performed as follows: 0.1 g of solid was dehydrated at 110–120 °C under vacuum. 0.015 g of TEPO dissolved in 5 mL of anhydrous *n*-pentane was added to the solid, and the mixture was stirred for 30 min under nitrogen, and then dried at 50 °C under vacuum. Solid-state NMR experiments were acquired on a Bruker Avance III spectrometer with a magnetic field of 9.4 T using a 4 mm double resonance probe operating at Larmor frequencies of 400.1 MHz and 161.9 MHz for ^1H and ^{31}P spins, respectively. ^{31}P $\{^1H\}$ MAS NMR spectra were recorded using a rotation speed of 12 kHz, a single excitation pulse width of 1.9 μs, employing a radio-frequency field strength of 56 kHz (60° flip angle) and 15 s recycle delay. TPPM-15 scheme was used for ^1H heteronuclear decoupling.

Catalytic tests

The batch catalytic experiments were performed in tubular glass reactors with pear-shaped bottoms and equipped with an appropriate PTFE-coated magnetic stirring bar and a valve. In a typical procedure, 0.33 M 5-(hydroxymethyl)-2-furfural (HMF, Aldrich, 99%) or furfuryl alcohol (FA, Aldrich, 99%), powdered catalyst (loading of 10 g_{cat} dm^{-3}), and 1 mL of ethanol (Scharlau, 99.9%) were added to the reactor at 110 °C. The reaction of fructose (0.33 M) in the presence of the catalyst (10 g_{cat} dm^{-3}) was carried out using a water–ethanol (3 : 7 v/v ratio) solvent mixture at 140 °C. The reaction mixtures were heated with a thermostatically controlled oil bath, under continuous magnetic stirring at 1000 rpm. Zero time (the instant the reaction began) was taken to be the instant when the micro-reactor was immersed in the oil bath. The heating time to reach 110–140 °C was 3–4 min. The initial reaction rates are based on conversion at 30 min reaction. The catalysts were separated after a 6 h batch run by centrifugation, washed with ethanol and then water. Prior to reuse the catalyst was separated from the reaction mixture by centrifugation and treated with aqueous H_2SO_4 (0.2 M) for 4 h at 30 °C. The catalysts were subsequently washed with water until the pH was neutral and dried at 85 °C overnight.

Comparisons of the catalytic results were made on the basis of similar mass of the catalyst, which is important in terms of practical application. The catalytic performances of the prepared composites were compared to those of a classical ion-exchange resin (Amberlyst™-15) and a large-pore zeolite (H-beta). The commercial cation-exchange resin Amberlyst™-15 (a macroreticular styrene–divinylbenzene copolymer bearing benzenesulfonic acid groups; FlukaChemika) was manually ground using an agate pestle and mortar and subsequently sieved to give a very fine powder with particle sizes of a few hundreds of nanometers (ascertained by SEM). Zeolite H-beta was prepared by calcination of commercial NH_4-form zeolite beta powder (NH_4BEA, Zeolyst, CP814; crystallites with a size of *ca.* 20–30 nm) at 550 °C for 10 h with a ramp rate of 1 °C min^{-1} in static air.

The evolution of the catalytic reactions was monitored by GC (for quantification of bioEs and FA) and HPLC (for quantification of HMF and fructose). Prior to sampling, the reactors were cooled to ambient temperature before opening and work-up procedures. The GC analyses were carried out using a Varian 3800 equipped with a capillary column (Chrompack, CP-SIL 5CB, 50 m × 0.32 mm × 0.5 μm) and a flame ionisation detector, using H_2 as the carrier gas. Authentic samples of the substrates were used as standards, and calibration curves were measured for quantification. The HPLC analyses were carried out using a Knauer Smartline HPLC Pump 100 and a Shodex SH1011 H^+ 300 mm × 8 mm (i.d.) ion exchange column (Showa Denko America, Inc., New York), coupled to a Knauer Smartline UV detector 2520 (254 nm for HMF), and a Knauer Smartline 2300 differential refractive index detector (for fructose); the mobile phase was 0.005 M aq. H_2SO_4 at a flow rate of 0.8 mL min^{-1}, and the column temperature was 50 °C. The

identification of the reaction products was accomplished by GCMS using a Trace GC 2000 Series (Thermo Quest CE Instruments) – DSQ II (Thermo Scientific), equipped with a capillary column (DB-5 MS, 30 m × 0.25 mm × 0.25 μm), using He as the carrier gas. Individual experiments were performed for a given reaction time and the presented results are the mean values of at least two replicates. The substrate (Sub) conversion (%) at reaction time t was calculated using the formula: 100 × [(initial concentration of Sub) − (concentration of Sub at time t)]/(initial concentration of Sub). The yield of the product (Pro) (%) at reaction time t was calculated using the formula: 100 × [(concentration of Pro at time t)/(initial concentration of Sub)]. The bioEs products were EL (ethyl levulinate) and 5EMF (5-(ethoxymethyl)-furfural) for fructose and HMF as substrates, and EL and 2EMF (2-(ethoxymethyl)-furan) for FA as the substrate.

Contact tests were carried out for C/SBA(45) and C/MCF(63) in order to study their stability. These experiments consisted of treating each composite in ethanol (ET) at 110 °C, or in water (WT) at 140 °C, for 24 h with stirring (the amount of solid added to the solvent was 10 g dm^{-3}). Afterwards, the solid was separated by centrifugation and washed using ethanol or water for the ET and WT treatments, respectively, and finally dried at 85 °C overnight. The ET treatment of C/SBA(45) and C/MCF(63) was carried out once giving the samples C/SBA(45)-ET and C/MCF(63)-ET, or twice giving C/SBA(45)-ET(2) and C/MCF(63)-ET(2), respectively. The solids obtained from the WT treatment of C/SBA(45) and C/MCF(63) are denoted C/SBA(45)-WT and C/MCF(63)-WT, respectively. The obtained materials were tested in the reaction of HMF under typical conditions, and characterised.

Acknowledgements

This work was partly financed by FEDER (Fundo Europeu de Desenvolvimento Regional) through COMPETE (Programa Operacional Factores de Competitividade) and by national funds through the FCT (Fundação para a Ciência e a Tecnologia) within the project CICECO - FCOMP-01-0124-FEDER-037271 (FCT ref. PEst-C/CTM/LA0011/2013). The FCT and the European Union are acknowledged for grants to P.A.R. (SFRH/BPD/79910/2011), M.M.A. (SFRH/BPD/89068/2012) and P.N. (SFRH/BPD/73540/2010) co-funded by MCTES and the ESF through the program POPH of QREN. We acknowledge the Portuguese National NMR Network (RNRMN), supported with funds from the FCT. BP Amoco Chemical Company is acknowledged for sponsoring P.V.W.'s postdoc grant. L.M. thanks the FCT for the FCT Investigator consolidation grant IF/01401/2013.

Notes and references

1 G. W. Huber, S. Iborra and A. Corma, *Chem. Rev.*, 2006, **106**, 4044–4098.
2 Y. Roman-Leshkov, C. J. Barrett, Z. Y. Liu and J. A. Dumesic, *Nature*, 2007, **447**, 982–985.
3 S. N. Naik, V. V. Goud, P. K. Rout and A. K. Dalai, *Renew. Sustainable Energ. Rev.*, 2010, **14**, 578–597.
4 J. J. Bozell and G. R. Petersen, *Green Chem.*, 2010, **12**, 539–554.
5 A.-L. Marshall and P. J. Alaimo, *Chem. – Eur. J.*, 2010, **16**, 4970–4980.
6 C. H. Zhou, X. Xia, C. X. Lin, D. S. Tong and J. Beltramini, *Chem. Soc. Rev.*, 2011, **40**, 5588–5617.
7 O. O. James, S. Maity, L. A. Usman, K. O. Ajanaku, O. O. Ajani, T. O. Siyanbola, S. Sahu and R. Chaubey, *Energy Environ. Sci.*, 2010, **3**, 1833–1850.
8 D. M. Alonso, J. Q. Bond and J. A. Dumesic, *Green Chem.*, 2010, **12**, 1493–1513.
9 R. Luque, A. Pineda, J. C. Colmenares, J. M. Campelo, A. A. Romero, J. Carlos Serrano-Ruiz, L. F. Cabeza and J. Cot-Gores, *J. Nat. Gas Chem.*, 2012, **21**, 246–250.
10 J. Zhang, S. Wu, B. Li and H. Zhang, *ChemCatChem*, 2012, **4**, 1230–1237.
11 A. Démolis, N. Essayem and F. Rataboul, *ACS Sustainable Chem. Eng.*, 2014, **2**, 1338–1352.
12 D. J. Hayes, *Catal. Today*, 2009, **145**, 138–151.
13 B. C. Windom, T. M. Lovestead, M. Mascal, E. B. Nikitin and T. J. Bruno, *Energy Fuels*, 2011, **25**, 1878–1890.
14 R. L. V. Mao, Q. Zhao, G. Dima and D. Petraccone, *Catal. Lett.*, 2011, **141**, 271–276.
15 E. Christensen, A. Williams, S. Paul, S. Burton and R. L. McCormick, *Energy Fuels*, 2011, **25**, 5422–5428.
16 M. Mascal and E. B. Nikitin, *Angew. Chem., Int. Ed.*, 2008, **47**, 7924–7926.
17 S. Dutta, S. De and B. Saha, *ChemPlusChem*, 2012, **77**, 259–272.
18 P. Che, F. Lu, J. Zhang, Y. Huang, X. Nie, J. Gao and J. Xu, *Bioresour. Technol.*, 2012, **119**, 433–436.
19 M. Balakrishnan, E. R. Sacia and A. T. Bell, *Green Chem.*, 2012, **14**, 1626–1634.
20 M. I. Alam, S. De, S. Dutta and B. Saha, *RSC Adv.*, 2012, **2**, 6890–6896.
21 P. Lanzafame, D. M. Temi, S. Perathoner, G. Centi, A. Macario, A. Aloise and G. Giordano, *Catal. Today*, 2011, **175**, 435–441.
22 L. Bing, Z. Zhang and K. Deng, *Ind. Eng. Chem. Res.*, 2012, **51**, 15331–15336.
23 K. S. Arias, S. I. Al-Resayes, M. J. Climent, A. Corma and S. Iborra, *ChemSusChem*, 2013, **6**, 123–131.
24 S. De, S. Dutta and B. Saha, *ChemSusChem*, 2012, **5**, 1826–1833.
25 X. Hu, R. Gunawan, D. Mourant, C. Lievens, X. Li, S. Zhang, W. Chaiwat and C.-Z. Li, *Fuel*, 2012, **97**, 512–522.
26 S. Saravanamurugan and A. Riisager, *Catal. Commun.*, 2012, **17**, 71–75.
27 G. J. M. Gruter and F. Dautzenberg, in US8338626 B2, 2012, p. 8.

28 G. J. M. Gruter and L. E. Manzer, in *US* 2010/0058650 A1, 2010, p. 7.
29 G. M. G. Maldonado, R. S. Assary, J. A. Dumesic and L. A. Curtiss, *Energy Environ. Sci.*, 2012, **5**, 8990–8997.
30 Z. Zhang, K. Dong and Z. Zhao, *ChemSusChem*, 2011, **4**, 112–118.
31 P. Neves, S. Lima, M. Pillinger, S. M. Rocha, J. Rocha and A. A. Valente, *Catal. Today*, 2013, **218**, 76–84.
32 J.-P. Lange, W. D. van de Graaf and R. J. Haan, *ChemSusChem*, 2009, **2**, 437–441.
33 P. Neves, M. M. Antunes, P. A. Russo, J. P. Abrantes, S. Lima, A. Fernandes, M. Pillinger, S. M. Rocha, M. F. Ribeiro and A. A. Valente, *Green Chem.*, 2013, **15**, 3367–3376.
34 R. J. Haan and J.-P. Lange, in *US* 8372164 B2, 2013, p. 4.
35 G. A. Kraus and T. Guney, *Green Chem.*, 2012, **14**, 1593–1596.
36 S. Saravanamurugan, O. N. Van Buu and A. Riisager, *ChemSusChem*, 2011, **4**, 723–726.
37 Y. Yang, M. M. Abu-Omar and C. Hu, *Appl. Energy*, 2012, **99**, 80–84.
38 A. S. V. d. S. Dias, G. J. M. Gruter and R.-J. V. Puttem, in *WO* 2012/091570 A1, 2012, p. 18.
39 G. J. M. Gruter, L. E. Manzer, A. S. V. d. S. Dias, F. Dautzenberg and J. Purmova, in *US* 2010/0081833 A1, 2010, p. 5.
40 G. J. M. Gruter, in *EP* 1834950 A1, 2007, p. 12.
41 G. J. M. Gruter, L. E. Manzer, A. S. V. d. S. Dias, F. Dautzenberg and J. Purmova, in *US* 8314260 B2, 2012, p. 5.
42 Y. Yang, C. Hu and M. M. Abu-Omar, *Bioresour. Technol.*, 2012, **116**, 190–194.
43 R. H. Lock and K. Reynolds, in *US* 2763665, 1956, p. 2.
44 G. Wang, Z. Zhang and L. Song, *Green Chem.*, 2014, **16**, 1436–1443.
45 X. Hu and C.-Z. Li, *Green Chem.*, 2011, **13**, 1676–1679.
46 H. Zhu, Q. Cao, C. Li and X. Mu, *Carbohydr. Res.*, 2011, **346**, 2016–2018.
47 A. J. Sanborn and S. J. Howard, in *US* 2009/0156841 A1, 2009, p. 23.
48 A. J. Sanborn, in *WO* 2006/063220 A2, 2006, p. 39.
49 X. Hu, L. Wu, Y. Wang, Y. Song, D. Mourant, R. Gunawan, M. Gholizadeh and C.-Z. Li, *Bioresour. Technol.*, 2013, **133**, 469–474.
50 H. Wang, T. Deng, Y. Wang, X. Cui, Y. Qi, X. Mu, X. Hou and Y. Zhu, *Green Chem.*, 2013, **15**, 2379–2383.
51 W. D. V. D. Graaf and J.-P. Lange, in *US* 7265239 B2, 2007, p. 6.
52 X. Wang, R. Liu, M. M. Waje, Z. Chen, Y. Yan, K. N. Bozhilov and P. Feng, *Chem. Mater.*, 2007, **19**, 2395–2397.
53 R. Liu, J. Chen, X. Huang, L. Chen, L. Ma and X. Li, *Green Chem.*, 2013, **15**, 2895–2903.
54 M. M. Antunes, P. A. Russo, P. V. Wiper, J. M. Veiga, M. Pillinger, L. Mafra, D. V. Evtuguin, N. Pinna and A. A. Valente, *ChemSusChem*, 2014, **7**, 804–812.
55 J. Ji, G. Zhang, H. Chen, S. Wang, G. Zhang, F. Zhang and X. Fan, *Chem. Sci.*, 2011, **2**, 484–487.
56 K. Nakajima, M. Okamura, J. N. Kondo, K. Domen, T. Tatsumi, S. Hayashi and M. Hara, *Chem. Mater.*, 2009, **21**, 186–193.
57 D. Nandan, P. Sreenivasulu, S. K. Saxena and N. Viswanadham, *Chem. Commun.*, 2011, **47**, 11537–11539.
58 S. Van de Vyver, L. Peng, J. Geboers, H. Schepers, F. de Clippel, C. J. Gommes, B. Goderis, P. A. Jacobs and B. F. Sels, *Green Chem.*, 2010, **12**, 1560–1563.
59 P. Valle-Vigón, M. Sevilla and A. B. Fuertes, *Appl. Surf. Sci.*, 2012, **261**, 574–583.
60 P. Gupta and S. Paul, *Green Chem.*, 2011, **13**, 2365–2372.
61 Q. Yue, M. Wang, J. Wei, Y. Deng, T. Liu, R. Che, B. Tu and D. Zhao, *Angew. Chem., Int. Ed.*, 2012, **51**, 10368–10372.
62 S. Suganuma, K. Nakajima, M. Kitano, D. Yamaguchi, H. Kato, S. Hayashi and M. Hara, *J. Am. Chem. Soc.*, 2008, **130**, 12787–12793.
63 W.-Y. Lou, Q. Guo, W.-J. Chen, M.-H. Zong, H. Wu and T. J. Smith, *ChemSusChem*, 2012, **5**, 1533–1541.
64 M. Toda, A. Takagaki, M. Okamura, J. N. Kondo, S. Hayashi, K. Domen and M. Hara, *Nature*, 2005, **438**, 178–178.
65 P. A. Russo, M. M. Antunes, P. Neves, P. V. Wiper, E. Fazio, F. Neri, F. Barreca, L. Mafra, M. Pillinger, N. Pinna and A. A. Valente, *J. Mater. Chem. A*, 2014, **2**, 11813–11824.
66 H. N. Pham, A. E. Anderson, R. L. Johnson, K. Schmidt-Rohr and A. K. Datye, *Angew. Chem., Int. Ed.*, 2012, **51**, 13163–13167.
67 R. Liu, Y. Shi, Y. Wan, Y. Meng, F. Zhang, D. Gu, Z. Chen, B. Tu and D. Zhao, *J. Am. Chem. Soc.*, 2006, **128**, 11652–11662.
68 A. C. Ferrari and J. Robertson, *Phys. Rev. B: Condens. Matter*, 2000, **61**, 14095–14107.
69 H. I. Lee, S. H. Joo, J. H. Kim, D. J. You, J. M. Kim, J.-N. Park, H. Chang and C. Pak, *J. Mater. Chem.*, 2009, **19**, 5934–5939.
70 L. Adams, A. Oki, T. Grady, H. McWhinney and Z. Luo, *Physica E*, 2009, **41**, 723–728.
71 J. F. Moulder, W. F. Strickle, P. E. Sobol and K. D. Bomben, *Handbook of X-ray Photoelectron Spectroscopy*, Perkin-Elmer Corporation (Physical Electronics), Eden Prairie, Minnesota, 1992.
72 W. H. Lee, J. Y. Kim, Y. K. Ko, P. J. Reucroft and J. W. Zondlo, *Appl. Surf. Sci.*, 1999, **141**, 107–113.
73 A. Zheng, S.-J. Huang, S.-B. Liu and F. Deng, *Phys. Chem. Chem. Phys.*, 2011, **13**, 14889–14901.
74 A. Zheng, S.-J. Huang, W.-H. Chen, P.-H. Wu, H. Zhang, H.-K. Lee, L.-C. de Menorval, F. Deng and S.-B. Liu, *J. Phys. Chem. A*, 2008, **112**, 7349–7356.
75 S. Saravanamurugan and A. Riisager, in *WO* 2014/02153 A1, 2014, p. 37.
76 Z. Zhang, Y. Wang, Z. Fang and B. Liu, *ChemPlusChem*, 2014, **79**, 233–240.

77 K. J. Zeitsch, *The Chemistry and Technology of Furfural and its Many By-Products*, Elsevier Science B. V., Amesterdam, The Netherlands, 2000.
78 P. S. Watson, J. A. Nuzum, D. B. Rohr, D. E. Newquist, C. T. Crawford and L. M. Bragg, *Furfuryl Alcohol from China, South Africa, and Thailand*, U.S. International Trade Commission, Washington, DC, 1994.
79 B. Liu, Z. Zhang and K. Huang, *Cellulose*, 2013, **20**, 2081–2089.
80 B. Liu and Z. Zhang, *RSC Adv.*, 2013, **3**, 12313–12319.
81 P. Pengthamkeerati, W. Kraewong and L. Meesuk, *Environ. Prog. Sustainable Energy*, 2014, 1–6.
82 D. Zhao, Q. Huo, J. Feng, B. F. Chmelka and G. D. Stucky, *J. Am. Chem. Soc.*, 1998, **120**, 6024–6036.
83 P. Schmidt-Winkel, W. W. Lukens, D. Zhao, P. Yang, B. F. Chmelka and G. D. Stucky, *J. Am. Chem. Soc.*, 1999, **121**, 254–255.
84 P. Schmidt-Winkel, W. W. Lukens, P. Yang, D. I. Margolese, J. S. Lettow, J. Y. Ying and G. D. Stucky, *Chem. Mater.*, 2000, **12**, 686–696.